Final published version of this article: Applied Surface Science, Volume 514, 26 February 2020, 145925
Available online: 27 February 2020
DOI: https://doi.org/10.1016/j.apsusc.2020.145925

Catalytic activity of $PtSn_4$: insights from surface-science spectroscopies

Gianluca D'Olimpio[1,*], Danil W. Boukhvalov[2,3], Jun Fujii[4], Piero Torelli[4], Andrea Marchionni[6], Jonathan Filippi[6], Chia-Nung Kuo[5], Raju Edla[4], Luca Ottaviano[1], Chin Shan Lue[5], Francesco Vizza[6], Silvia Nappini[4], and Antonio Politano[1,7,*]

1 Department of Physical and Chemical Sciences, University of L'Aquila, via Vetoio, 67100 L'Aquila (AQ), Italy
2 College of Science, Institute of Materials Physics and Chemistry, Nanjing Forestry University, Nanjing 210037, P. R. China
3 Theoretical Physics and Applied Mathematics Department, Ural Federal University, Mira Street 19, 620002 Ekaterinburg, Russia
4 Consiglio Nazionale delle Ricerche (CNR)- Istituto Officina dei Materiali (IOM), Laboratorio TASC in Area Science Park S.S. 14 km 163.5 34149 Trieste, Italy
5 Department of Physics, National Cheng Kung University, 1 Ta-Hsueh Road, 70101 Tainan, Taiwan
6 Consiglio Nazionale delle Ricerche (CNR)- Istituto di Chimica dei Composti OrganoMetallici (ICCOM), Area della Ricerca di Firenze, via Madonna del Piano 10, 50019 Sesto Fiorentino, Italy
7 Consiglio Nazionale delle Ricerche (CNR)- Istituto di Microelettronica e Microsistemi (IMM), VIII strada 5, 95121 Catania, Italy

Abstract

Bulk $PtSn_4$ has recently attracted the interest of the scientific community for the presence of electronic states exhibiting Dirac node arcs, enabling possible applications in nanoelectronics. Here, by means of surface-science experiments and density functional theory, we assess its suitability for catalysis by studying the chemical reactivity of the (010)-oriented $PtSn_4$ surface toward CO, H_2O, O_2 molecules at room temperature and, moreover, its stability in air. We demonstrate that the catalytic activity of $PtSn_4$ is determined by the composition of the outermost atomic layer. Specifically, we find that the surface termination for $PtSn_4$ crystals cleaved in vacuum is an atomic Sn layer, which is totally free from any CO poisoning. In oxygen-rich environment, as well as in ambient atmosphere, the surface termination is a SnO_x skin including SnO and SnO_2 in comparable amount. However, valence-band states, including those forming Dirac node arcs, are only slightly affected by surface modifications. The astonishingly beneficial influence of surface oxidation on catalytic activity has been demonstrated by electrocatalytic tests evidencing a reduction of the Tafel slope, from 442 down to 86 mV dec^{-1}, whose origin has been explained by our theoretical model. The use of surface-science tools to tune the chemical reactivity of $PtSn_4$ opens the way toward its effective use in catalysis, especially for hydrogen evolution reaction and oxygen evolution reaction.

* Corresponding authors:

gianluca.dolimpio@graduate.univaq.it (Gianluca D'Olimpio),

antonio.politano@univaq.it (Antonio Politano)

Keywords: X-ray photoelectron spectroscopy, hydrogen evolution reaction; surface science; high-resolution electron energy loss spectroscopy; oxidation

Introduction

In the last decade, the advent of topological materials has triggered the interest of a broad community mainly for fundamental research [1-7]. However, recently, topological materials have emerged as potential candidates for catalysis, as reported for topological insulators [8] and, successively, for Weyl [9] and Dirac [10] semimetals. Among the various topological materials, Pt-based topological systems are particularly relevant for catalytic applications, due to the wide use of Pt in several catalytic reactions, including hydrogen evolution reaction [11], oxygen evolution reaction [12], carbon monoxide oxidation [13], water-gas shift [13] and water splitting [14]. However, the high cost (>30 US $/g) [15] and the restricted obtainability [16] of Pt make unavoidable to search economic and Earth-abundant potential alternatives. A solution could be using Pt-alloys to reduce Pt content, which also enable the exploitation of strain and ligand effects to enhance their chemical reactivity [17]. Previously, the use of Pt-Sn polycrystalline alloys in electrochemistry has been explored for several reactions [18-21], although such alloys are mainly used for soldiery [22], electronic interconnections [23], jewelry [24], and dentistry [24]. Specifically, Pt-Sn alloys are employed for the catalytic process leading to alkanes-alkenes conversion [25] and, moreover, as anodes with improved resistance to CO poisoning compared to pure Pt [26], due to (i) the reduced saturation coverage of CO [27] and (ii) the lower heat of adsorption for CO on Pt sites (95 vs 180 kJ/mol) [28].

Among Pt-Sn binary alloys, five stoichiometric compounds Pt_3Sn, PtSn, Pt_2Sn_3, $PtSn_2$, and $PtSn_4$ exist [29]. Recently, Dirac node arc was found in $PtSn_4$ single crystals, i.e. closed loops formed by Dirac nodes in the momentum domain [30]. From transport experiments in Ref. [31] one can estimate an electrical conductivity at room temperature of $2.5 \cdot 10^5$ S/m, which is increased by a 10^3 factor at T=2 K. Thus, $PtSn_4$ can be suitably used as electrode in electrochemistry, also in consideration of the carrier density $n \simeq 2.6 \times 10^{28}$ m^{-3}. Very recently, the suitability of $PtSn_4$ for hydrogen evolution reaction (HER) has been evidenced [32], although the mechanism ruling HER activity remains largely uncertain.

Large-size $PtSn_4$ single crystals can be efficiently grown by flux method [31]. The recent achievement of $PtSn_4$ nanoparticles [33] signifies a further advantage in the prospect of large-scale catalytic devices, as well as the reduced cost of $PtSn_4$ (~9 US $/g) compared to pure Pt. However, the control of surface phenomena (surface termination, chemical reactivity, surface reconstruction) is required for the exploitation of $PtSn_4$ in electrocatalysis and nanoelectronics. It is important to note that also the emergence itself of Dirac node arcs is associated to the surface states [30] and it is strictly connected to the surface termination. Unfortunately, surface-science investigations on $PtSn_4$ are missing yet. The lack of information about surface properties represents a severe hurdle to understand and tailor surface catalysis based on $PtSn_4$.

Here, we combine high-resolution X-ray photoelectron spectroscopy (XPS), scanning tunneling microscopy/spectroscopy (STM/STS) and high-resolution electron energy loss spectroscopy (HREELS) with density functional theory (DFT) to clarify the key features of chemical reactivity of $PtSn_4$ surfaces toward ambient gases. We demonstrate that the termination of the as-cleaved surface is an atomic layer of Sn exhibiting a high CO tolerance, with no trace of CO adsorption. However, the surface is unstable in oxygen environment and in air, with the emergence of a SnOx skin involving Sn(II) and Sn(IV) species. We also demonstrate that valence-band electronic states, including those forming the Dirac node arcs, are robust against surface oxidation. Finally, we assess catalytic performance of $PtSn_4$ surfaces toward HER and oxygen evolution reaction (OER) by both theory and electrochemical tests, finding that surface oxidation is beneficial for catalysis.

Methods

Single-crystal growth and cleavage

Self-flux method was used to synthesize single crystals of $PtSn_4$. High-purity Pt foil (99.99%) and Sn ingots (99.999%) were mixed in the ratio of 1:25 and sealed in an evacuated quartz tube. The mixed elements were heated to 600 °C for 6 hours, dwelled for 10 hours, quickly cooled to 350 °C

in 5 hours, and then slowly cooled at a rate of 1°C/h to 250 °C. Afterwards, the excess Sn flux was removed by centrifugation and then etched in concentrated hydrochloric acid. The structure of the grown crystals was examined by X-ray diffraction (Bruker D2 PHASER) using Cu Kα radiation and Laue diffraction (Photonic Science) at room temperature. The sharp features in the XRD pattern and clear spots in the Laue pattern suggest high crystalline quality (Fig. 1 a-b). The cleavage of $PtSn_4$ was conducted by post-method in ultra-high vacuum through the natural cleavage plane, coinciding with the (010) orientation. Surface cleanliness was checked by XPS and vibrational spectroscopy, while surface crystalline order was checked by STM and low-energy electron diffraction.

XPS

XPS experiments were performed at the High-Energy branch of the Advanced Photoelectric Experiments beamline (APE-HE) of the Elettra Synchrotron, Trieste, Italy. XPS spectra were acquired with an Omicron EA125 hemispherical electron energy analyzer, with the sample at room temperature and in normal emission condition. The linearly polarized light was impinging on the sample forming an angle of 45 degrees with respect to the normal to the surface. To evaluate BEs of core levels, a Shirley background was subtracted from XPS spectra. Pt-4f and Sn-3d core-level spectra were analyzed by using a Doniach–Sunjic function [34], convoluted with a Gaussian line-shape to account for experimental resolution, inhomogeneity, and temperature-derived broadening. Conversely, for O-1s core level we adopted Voigt line-shapes. Under our experimental conditions, we had any evidence of beam-induced damage. Gas inlet of carbon monoxide, water and oxygen was performed by using leak valves at a common exposure at a pressure of 10^{-4} mbar for 10 min, corresponding to 450 kL (1 L=$1 \cdot 10^{-6}$ torr·s).

STM/STS

STM and STS were conducted using a home-built room-temperature ultra-high vacuum (UHV) STM apparatus connected to the APE beamline with UHV transfer system, which enables to measure STM/STS for the same sample for the electron spectroscopy and LEED. In-situ cleaned W tip

was used for both STM and STS. The STM topography image was taken with constant current mode. The bias voltage was applied on the sample. Data analysis was performed with the WSxM software [35].

HREELS

HREELS experiments were carried out with a Delta 0.5 spectrometer by Specs GmbH, Germany. The impinging energy is 3.5 eV. Spectra were recorded in specular direction, with an incidence angle of 55° with respect to the sample normal.

Electrochemical tests

Electrochemical experiments were conducted in a common three electrodes glass cell equipped with Pt wire as counter electrode and Ag/AgCl/KCl sat as reference electrode and all the potentials were referred to the RHE. Equipment was cleaned with a mix of water and 2-propanol and rinsed several times with ultrapure water (18.2 MΩ). A 0.05 M solution of sulfuric acid (99.9%, Sigma Aldrich) in ultrapure water was used as electrolyte. The electrochemical experiments were conducted with a Priceton Applied Research (PAR) PARSTAT 2277 potenziostat galvanostat. All current measurements were normalized to the geometric surface area of each electrode. CVs experiments were conducted at 50 mV s^{-1}, otherwise stated. Slow linear sweep experiments to obtain the Tafel slope were conducted at 1 mV s^{-1}.

DFT calculations

The atomic structure and energetics of various configurations was studied by DFT using the QUANTUM-ESPRESSO code [36] and the GGA–PBE [37], taking into account van der Waals forces correction[38]. For all calculations ultrasoft pseudopotentials were used [39]. Energy cutoffs

of 25 and 400 Ry for the plane-wave expansion of the wave functions and the charge density were used, respectively. Atomic structure of $PtSn_4$ was taken from experimental results in Ref. [40], while the atomic structure of PtC is assumed to be the one in the theoretical model in Ref. [41]. Total energies of gases were calculated for the single molecule in empty box. The total energy of Pt for Pt-rich conditions is defined by the formula: $E(Pt) = 4E(Sn) – E(PtSn_4)$, where E(Sn) is the total energy of bulk metallic tin. For computing the total energy of Sn, a similar procedure was used. The enthalpy of reaction is defined as difference in calculated total energies of products and reactant. Thus, negative enthalpy corresponds with exothermic reactions.

Physisorption enthalpies were calculated by the standard formula:

$$\Delta H_{phys} = [E_{host+mol} - (E_{host} + E_{mol})],$$

where E_{host} is the total energy of pristine surface, and E_{mol} is the energy of the single molecules of selected species in empty box. In the case of water adsorption, we only considered the gaseous phase. Decomposition energy is defined as difference between the total energy of the system with adsorbed molecule and the total energy of same system after decomposition of the same molecule on the surface. For the case of physisorption, we also evaluated differential Gibbs free energy by the formula:

$$\Delta G = \Delta H - T\Delta S,$$

where T is the temperature and ΔS is the change of entropy of adsorbed molecule, which was estimated considering the gas→liquid transition by the standard formula:

$$\Delta S = \Delta H_{vaporisation}/T,$$

where $\Delta H_{vaporization}$ is the measured enthalpy of vaporization. HER were calculated for standard hydrogen electrode, while OER was calculated for acidic environment (the value of the overpotential is 1.23 eV).

Results and Discussion

Single crystals of $PtSn_4$ have a preferential (010) cleavage plan, as evidenced by room-temperature x-ray diffraction (XRD) pattern (Fig. 1a). Lattice constants evaluated from XRD are $a =$ (6.405±0.002) Å, b=(11.371±0.002) Å, c=(6.372±0.002) Å, consistently with previous reports in literature [42].

The determination of the surface termination is crucial in order to achieve control over surface phenomena, since the outermost layer of the crystal mostly determines surface chemical reactivity [43]. Especially, there are three possible surface terminations that can be realized for the natural cleavage plane. The first possibility could be a Sn-terminated surface, where the Pt subsurface layer is placed between two Sn layers (2Sn-termination), as in the $PtSn_4$ bulk crystal, while the second possibility is a Pt-terminated surface with nearest Pt atoms distant 0.45 nm. A third possibility is a 1Sn-termination, with a single Sn atomic surface layer on top of an underlying layer of Pt atoms.

To evaluate the compositional (Sn/Pt ratio) depth profile of $PtSn_4$, XPS experiments were performed at various photon energies (800, 400 and 300 eV) and, moreover, at various emission angles (65,55 and 45 degrees) with a photon energy of 400 eV. The energy-dependent XPS analysis indicated an increased Sn/Pt ratio at decreasing photon energy, i.e. in conditions with higher surface sensitivity. Congruently, the angle-dependent photoemission revealed an increased ratio of Sn/Pt going from normal (90°) to grazing (45°) emission angle, i.e. in conditions with higher surface sensitivity. Therefore, both energy- and angle-dependent analysis indicate the occurrence of a Sn-terminated surface. The respective photon energy and angle-dependent values of the Sn/Pt ratio are reported in Table 1.

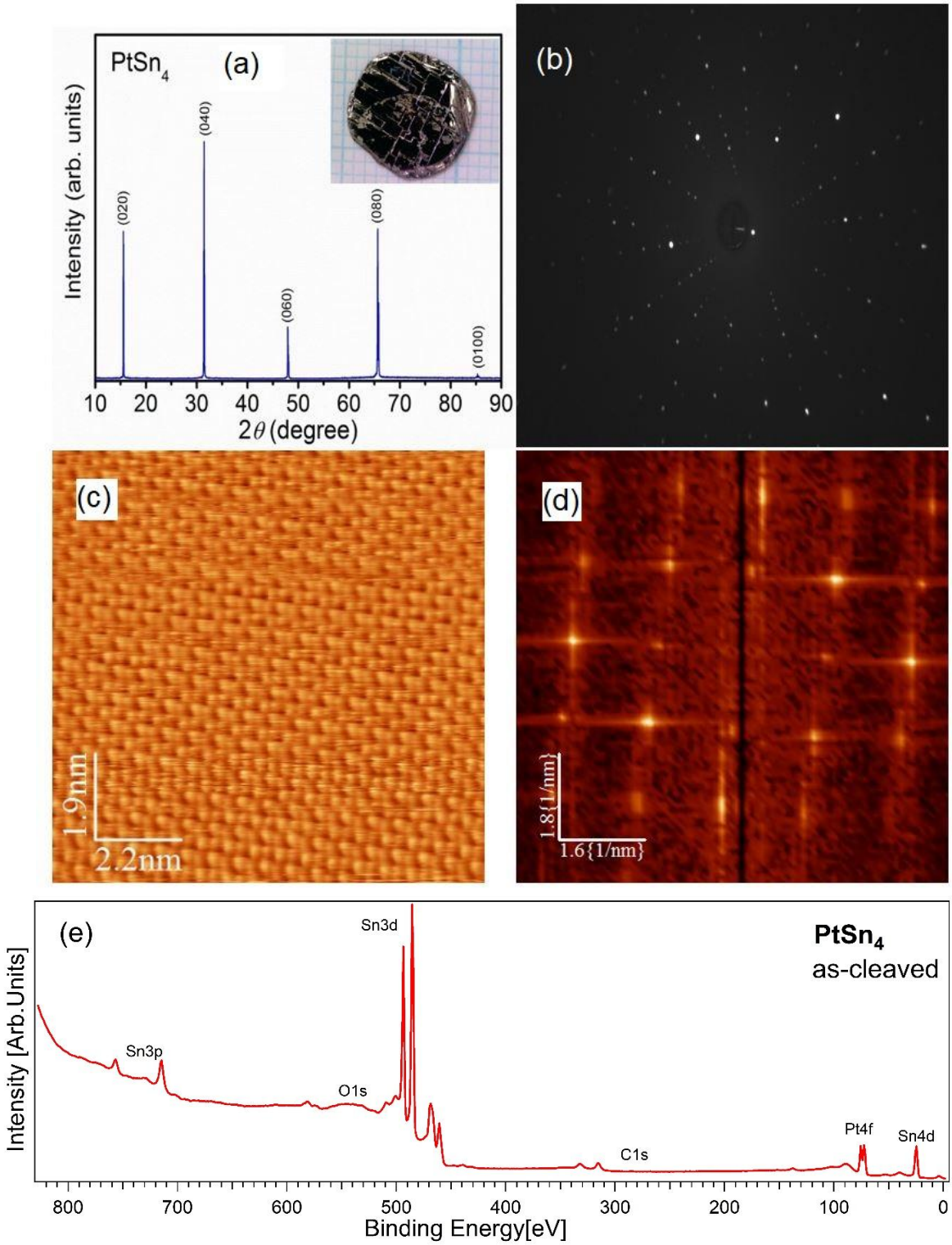

Figure 1. (a) Room-temperature single-crystal x-ray diffraction pattern from the (010) plane of $PtSn_4$. The inset shows a photograph of an as-grown $PtSn_4$ single crystal. (b) Laue diffraction image taken along the (010) direction. (c-d) Atomically-resolved STM and FFT image of $PtSn_4$. The constant current image was taken at a sample bias voltage of +620mV and a tunneling current of 0.7nA. (e) XPS survey scan of an as-cleaved sample, clearly showing the cleanliness of the surface (especially, no C-1s and O-1s components). The photon energy is 800 eV.

Table 1. Values of the Sn/Pt ratio obtained for an as-cleaved $PtSn_4$ sample evaluated by XPS spectra acquired using different (i) photon energy (800, 400 and 300 eV) and (ii) emission angles (65, 55 and 45 degrees)

Photon Energy	**Geometry**	**Sn/Pt ratio**
900 eV	Normal Emission	4.3±0.6
400 eV	Normal Emission	5.4±0.8
300 eV	Normal Emission	6.3±0.9
400 eV	90° Emission	4.3±0.7
400 eV	65° Emission	5.0±0.7
400 eV	55° Emission	5.7±0.8
400 eV	45° Emission	5.3±0.8

Atomic-resolution images acquired by scanning tunneling microscopy (STM, Fig. 1 c) and their corresponding fast-Fourier transform (FFT, Fig. 1d) are consistent with the square lattice. According to STM, the surface unit cell is 0.33 x 0.33 nm, matching surface lattice of a Sn termination.

The analysis of core-level spectra measured with XPS is crucial in order to assess surface chemical reactivity of $PtSn_4$. Firstly, it is worth noticing that the analysis of survey XPS spectrum of $PtSn_4$ (Fig. 1e) ensures that surface cleanliness is obtained after cleavage in UHV, as evidenced by the absence of signal from C-1s and O-1s core levels in the as-cleaved sample. Figure 2 (top panel) shows Pt-4f and Sn-3d core levels measured for the as-cleaved surface and after exposure to 450 kL (1 $L=10^{-6}$ torr·s) of O_2, CO and H_2O respectively. Specifically, Pt-4f core levels of the as-cleaved $PtSn_4$(010) surface are split by spin-orbit coupling in two components centered around binding energies (BE) of ~75.3 ($4f_{5/2}$) and ~72.0 eV ($4f_{7/2}$). These values are shifted by +1.0 eV compared to Pt(111) [44-46]. We ascribe the blue-shift of the Pt-4f components with respect to pure Pt surfaces to the presence of Pt-Sn bonds, as previously observed also on other Pt-based alloys [47, 48]. According to the results of the systematic study on Pt-based alloys in Ref. [48], such a blue-shift com-

pared to pure Pt is typical of CO-tolerant electrodes, which suffer less CO poisoning than pure Pt as a consequence of the reduced electron donation from the Pt-d bands to the 2π* orbital of CO.

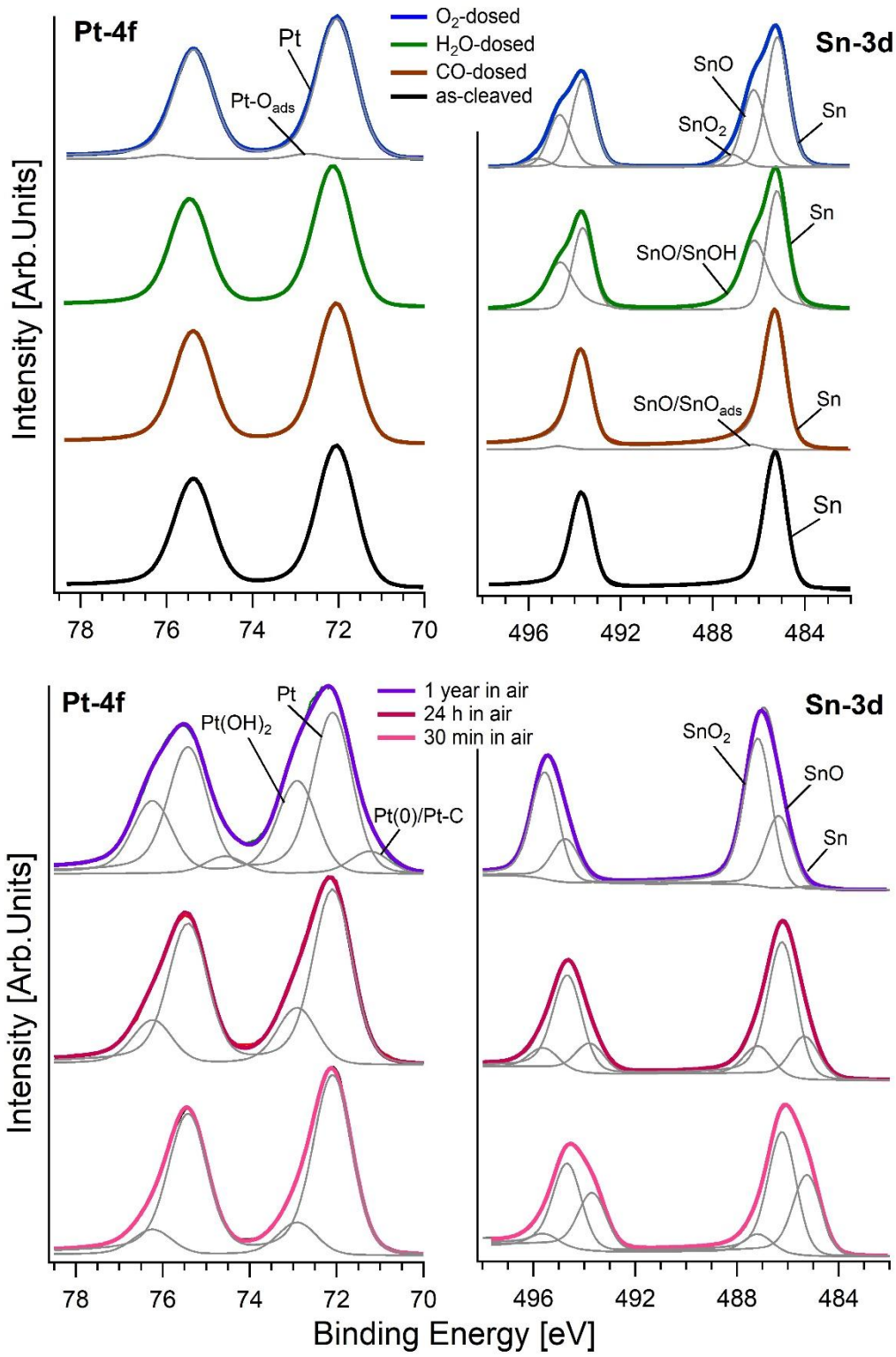

Figure 2. Core-level spectra for (top panel) Pt-4f and Sn-3d for as-cleaved, CO-dosed, H_2O-dosed, and O_2-dosed $PtSn_4$ and (bottom panel) $PtSn_4$ exposed to air for 30 minutes, 24 hours, and one year. The photon energy is 800 eV and the spectra are normalized to the maximum.

In the as-cleaved sample, Sn-3d core level has a doublet with BEs centered at 485.2 eV ($3d_{5/2}$) and 493.7eV ($3d_{3/2}$), which can be ascribed to Sn atoms in the bulk [49-51] (Fig. 2, top panel).

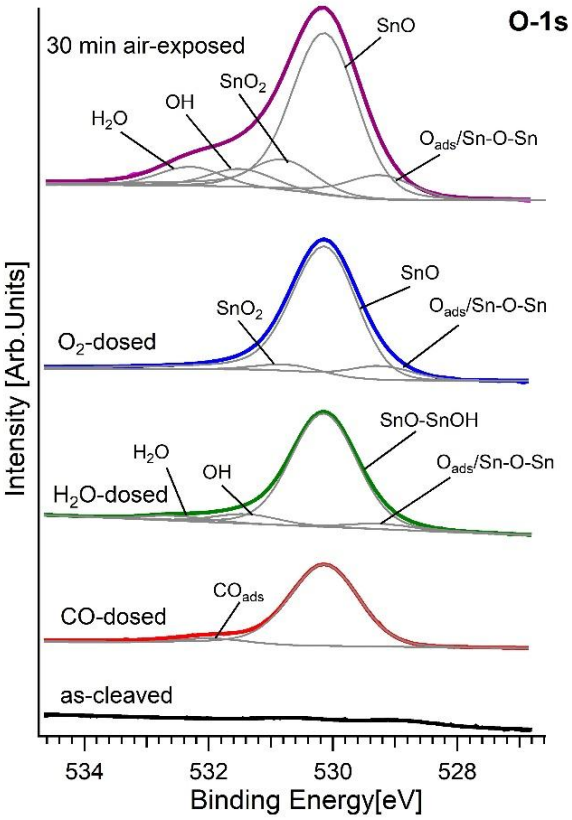

Figure 3. O-1s core-level spectra for as-cleaved, CO-dosed, H_2O-dosed, O_2-dosed and air-exposed (30 minutes) $PtSn_4$. The photon energy is 800 eV.

When $PtSn_4$ is exposed to H_2O and O_2, both oxidation and water adsorption selectively involve only Sn atoms. Especially, no additional features in Pt-4f core levels are reported, except negligible contribution from Pt-O_{ads} (4 %) in O_2-dosed sample [52, 53] (Fig. 2). Sn-3d core-level spectra (Fig. 2) show the presence of a component ascribable to SnO/Sn-OH species (BE of ~486.2 eV) in H_2O-dosed sample[50, 54, 55], while a further component due to SnO_2 (BE of ~487.2 eV) [50] is observed in O_2-dosed sample. In H_2O-dosed sample, oxide and hydroxide components (SnO/Sn-OH) are ~25% of Sn-3d total area. In the case of O_2-dosed $PtSn_4$, the oxidation is dominated by both SnO (35%) and SnO_2 (6%) components.

Previously, by means of XPS it was concluded that $Pt_3Sn(111)$ is converted into $SnOx/Pt_3Sn$ at high pressures (as high as 0.067 mbar [50]) of O_2, due to segregation and the following formation of a surface tin-oxide phase [50]. Such an interface also promotes low-temperature CO oxidation [56],

with a reaction kinetics enhanced compared to Pt(111) and (111)-oriented Pt-skin/Pt_3Sn. The presence of a high Sn content in $PtSn_4$, as compared to other Pt-Sn alloys, enables the stable chemisorption of O at room temperature. For the sake of completeness, it is worth mentioning that Pt-Sn interactions possibly lead to the spillover of O from Sn to Pt sites [57], as evidenced by small – albeit noticeable – changes (4 % contribution) in the Pt-4f spectra.

Through quantitative XPS analysis, we have calculated the thickness of the tin-oxide layer in H_2O-dosed and O_2-exposed samples to be around 6.6±0.9 and 7.2±1.0 Å, respectively. Thus, we can infer that the bulk $PtSn_4$ is protected by the sub-nanometric tin-oxide layer, that have a negligible effect only on first atomic layer of Pt.

For both H_2O- and O_2-dosed $PtSn_4$, we find (Fig. 3) one O-1s main component at ~530.3 eV and minor components at 529.6 eV ascribable to the formation of SnO/Sn-OH and SnO species[50, 58], congruently with the corresponding component at ~486.2[50] eV in the Sn-3d spectrum, and to Sn-O-Sn bonds arising in the early stages of tin-oxide formation [50, 54] respectively. A small component at a BE of ~531.5eV can be associated to the chemisorption of OH or H_2O species [59-61] in H_2O-exposed $PtSn_4$ surface. O_2-dosed sample also shows an additional component at 530.9 eV in O-1s spectrum ascribable to the formation of SnO_2 .[50] The same contribution is also observed in the corresponding Sn-3d core level spectrum in Fig. 2, where the small component at 487.2 eV can be assigned to SnO_2 (5% of the total spectral area) [62]. It should be mentioned that a strong H_2O-induced band bending has been previously reported for water adsorption on SnO_2 [63], as a consequence of the formation of surface hydroxyls.

We have also exposed the as-cleaved $PtSn_4$ directly to ambient atmosphere. The analysis of Sn-3d and O-1s core levels (Figs. 2 and 3) clearly shows the resemblance with the case of the O_2-dosed sample. The components arising from SnO and SnO_2, as well as the water-derived contamination of the oxide layer, are all increased in intensity in the air-exposed $PtSn_4$ surface compared to the cases of surface modification by the gas exposures in vacuum reported in Fig. 2. The Pt-4f spectrum ac-

quired for the $PtSn_4$ surface kept 30 minutes in air shows a new component at BE 72.95 eV ascribable to $Pt(OH)_2$ [64, 65] or Pt-O units[50] in an early stage oxidation of Pt atoms . The $Pt(OH)_2$/Pt-O units component was not observed in the sample exposed to gases in vacuum (Fig. 2), indicating that only air exposure can induce changes in Pt oxidation status.

It is also worth mentioning that the time evolution of O-1s during air exposure is consistent with the picture emerging from the analysis of Pt-4f and Sn-3d core levels.

We have also assessed the chemical reactivity toward CO, which is particularly relevant considering that Pt alloys usually show high reactivity toward CO implying passivation of active sites [66, 67]. Correspondingly, electrodes for electrocatalysis based on Pt alloys suffer CO poisoning [68-70], especially relevant for the case of methanol oxidation reaction [71, 72]. Core-level spectra acquired after having exposed to CO the $PtSn_4$ surface (Fig. 2, top panel) demonstrate the perfect tolerance toward CO-induced surface poisoning, in spite of the presence of Pt atoms in the crystal structure. In fact, no changes in the line shape of Pt-4f spectrum was detected. An accurate investigation of Sn-3d core levels reveals a small contribution (8% of the total spectral area) at ~486.2 eV for Sn-$3d_{5/2}$, which can be assigned to SnO species resulting from the early stage of tin-oxide formation (SnO/SnO_{ads}), arising from the decomposition of CO molecules at Sn sites in the nearness of edges [50] . Correspondingly, the O-1s core level (Fig. 3) shows SnO contribution at ~530.3 eV[50].

However, surface vibrational spectroscopies have higher sensibility to CO adsorption with respect to XPS [73, 74]. Thus, in order to strengthen conclusions from XPS analysis, we have carried out a vibrational investigation by HREELS (Fig. 4a), which fully confirms the CO tolerance of $PtSn_4$. In particular, the featureless spectrum in the region of C-O stretching in the 210-255 meV range (see Ref. [75] for a review of vibrational investigations on CO/metals) represents an unambiguous demonstration that $PtSn_4$ could represent a perfectly CO tolerant electrode. Definitely, the coverage of CO can be estimated to be ~10^{-3} ML (with ML meaning "monolayer") by considering both

HREELS spectra in Fig. 4a and O-1s in Fig. 3. Remarkably, the vibrational spectrum of the CO-dosed surface is characterized by a feature at 60 meV accompanied by a weak peak at 120 meV, that can be assigned to the SnO optical phonon at 60 meV [58] and its first-order replica, consistently with dissociative CO adsorption at defect sites. The same features are present also for direct exposure to O_2. The negligible dependence on the amount of the CO dose indicates fast saturation of active sites, further supporting the occurrence of dissociation at defect sites. For the sake of comparison, we report in Fig. 4b the vibrational spectra of other Pt-based systems saturated with CO (with less than 10 L), i.e. Pt-skin-terminated $Pt_3Ni(111)$ and Pt(111), for which we instead observe the saturation of on-top and three-fold hollow sites with CO (C-O stretching features at 257 and 230 meV, respectively) and the CO-substrate stretching at 56 meV, similarly to previous reports on the same systems [66].

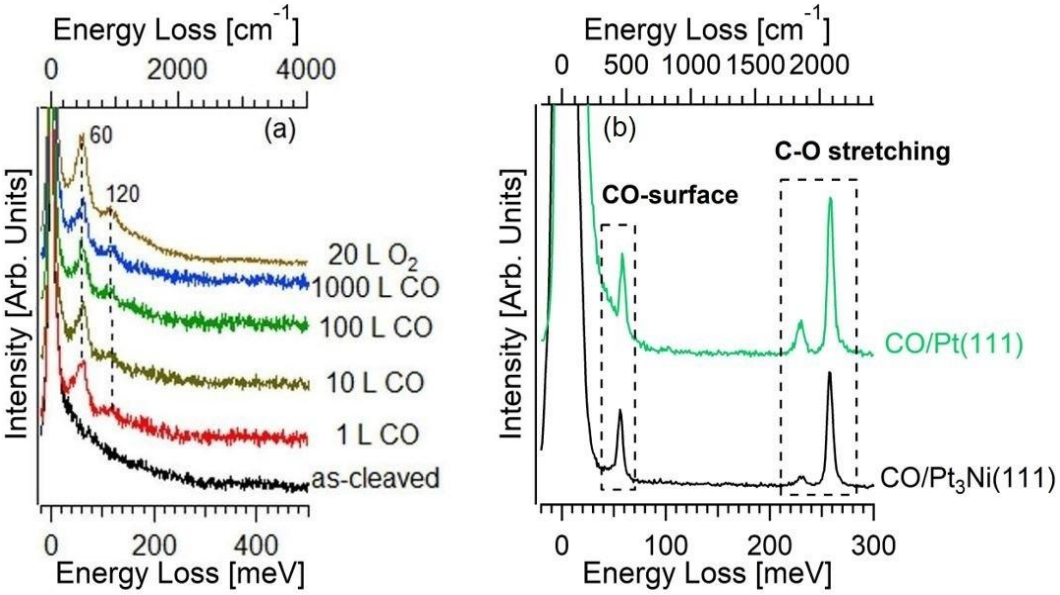

Figure 4. (a) HREELS spectra for pristine $PtSn_4$ and the same surface modified by the exposure to different amounts (1-1000 L) of CO and to 20 L of O_2 at room temperature. (b) HREELS spectra for the CO-saturated Pt(111) and $Pt_3Ni(111)$ surfaces, achieved for less than 10 L in both cases. Both measurements and exposures have been carried out at 300 K. All spectra were normalized to the intensity of the elastic peak. Spectra have been recorded in specular geometry (incidence angle 55° with respect to the sample normal) and with a primary electron beam energy of 4 eV.

The eventual effects of chemisorption and oxidation on electronic properties were assessed by measuring the valence band (Fig. 5), finding that surface treatments and air exposure only produced minimal effects. Being topological properties connected to Dirac node arcs located in the nearness

of the Fermi level [30], it is evident that this finding implies the robustness of the topological states of the bulk crystal of $PtSn_4$, which are not modified by the presence of the tin-oxide skin. However, Dirac node arcs are expected to be quenched, since they arise from dangling bonds in the surface layer, which are not present in the tin-oxide skin.

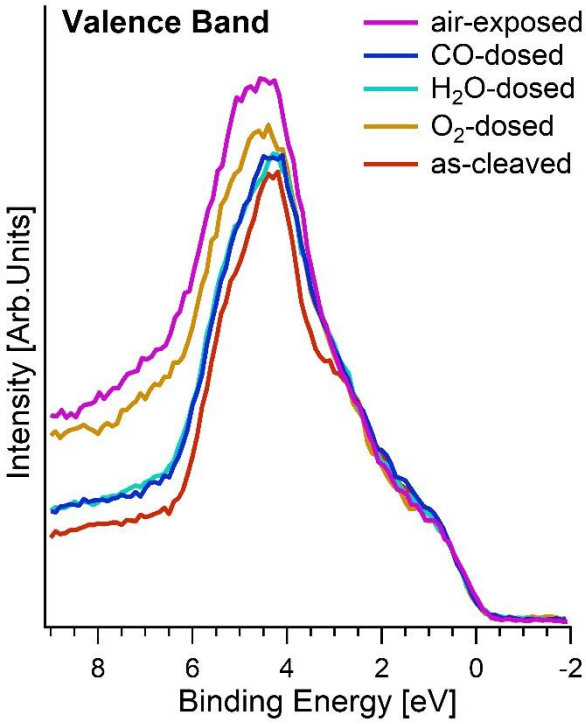

Figure 5. Valence-band spectra normalized to the Fermi edge for as-cleaved, CO-dosed, H_2O-dosed, O_2-dosed and air-exposed $PtSn_4$. The photon energy is 800 eV.

The analysis of surface chemical reactivity in Figs. 2-5 has been complemented by a joint theoretical and experimental assessment of the catalytic activity toward HER and OER.

In our model, we checked the standard pathway of HER, i.e. (i) Volmer ($H^+ + e^- \rightarrow H_{ads}$) and, successively, (ii) Heyrovsky ($H_{ads} + H^+ + e^- \rightarrow H_2$) reactions. In Fig. 6, the atomic structures used for theoretical modelling are visualized. In particular, we also considered a possible Pt termination, with the aim to assess eventual capabilities enabled by different synthesis methods (e.g., epitaxial growth).

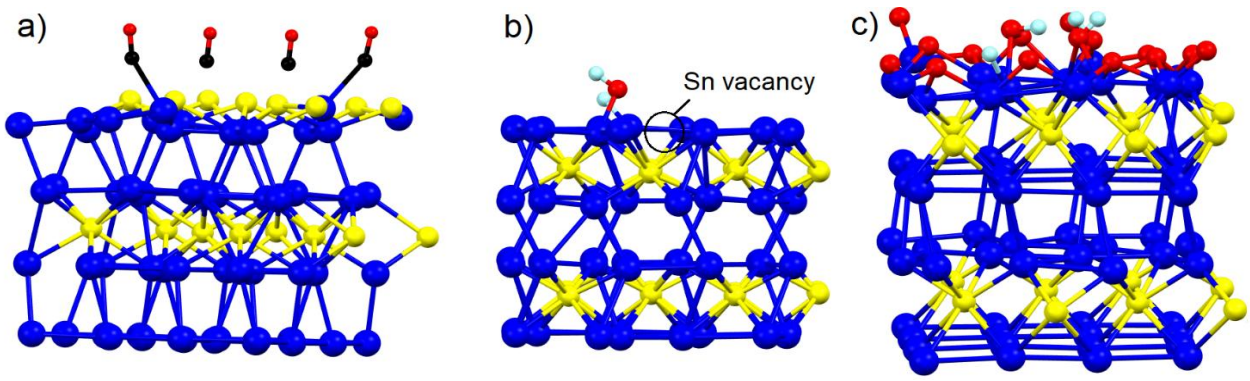

Figure 6. Optimized atomic structure of (a) the physisorption of CO molecules on Pt-terminated surface at saturation coverage and (b) decomposition of water molecule on 1Sn-terminated surface with one Sn vacancy and (c) four hydrogen atoms adsorbed on oxidized 1Sn-terminated surface (Volmer step of HER).

Calculations demonstrate favorability of hydrogenation of $PtSn_4$ surface for all types of considered termination. This makes the second step of HER (Heyrovsky reaction) rather energetically unfavorable (Fig. 7a), in contrast with experimental results. Therefore, we considered another opportunity: combination of (i) Volmer and (ii) Tafel steps. In the case of oxidized 1Sn-surface, hydrogen atoms bind to oxygen atoms with the formation of hydroxyl groups (Fig. 6c). In this case, Tafel step does not represent the migration of the adatom on the surface but instead the migration of hydrogen from one oxygen atom to another. As the distance between oxygen atoms in oxidized 1Sn-surface is about 0.2 nm (less than the distance between surface atoms in any metal) and considering doping from Pt-sublayer, the energy cost of hydrogen migration results to be only 0.2 eV, i.e. comparable with the energy cost of Heyrovsky reaction for Pt(111).

We have also modelled OER for unoxidized surfaces of $PtSn_4$. Similarly to Pt(111) and other metallic catalysts, the rate of this reaction determined by the energy cost of the third step (formation of -OOH groups on substrate). In the case of Pt-terminated surface, the energy cost of this step is smaller than for pure Pt (~1.0 eV vs ~1.3 eV, respectively), whereas for 1Sn-surface it is slightly higher (~1.5 eV). Considering that (i) the energetics of OER over 1Sn-surface is comparable with platinum and (ii) this surface displays tolerance toward CO poisoning, we can propose further ex-

perimental evaluation of $PtSn_4$ as catalyst for OER and oxygen reduction reaction (ORR).

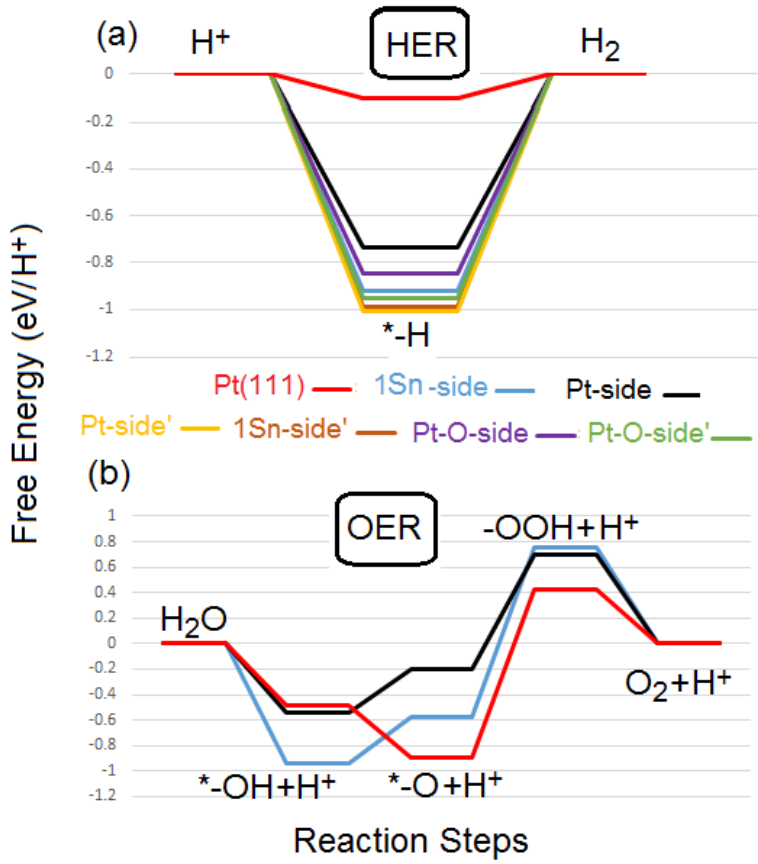

Figure 7. Free energy diagrams for hydrogen (a) and oxygen (b) evolution reactions on various surfaces of $PtSn_4$. The data for Pt(111) are adopted from the Ref.[12] Results for whole hydrogen coverage of Pt-terminated surface are marked by a prime symbol (').

Notably, experimentally the similarity in HER performance with the case of Pt only appears whenever the $PtSn_4$ surface is exposed to potential higher than 1.035 V vs RHE. To elucidate this unexpected behaviour, we reported (Fig. 8a) the current density of the backwards scan (from 0.05 to -0.05 V vs RHE) of the stable cycle as a function of the upper inversion potential value. The lower inversion potential remained the same for all these measurements (-0.1 V vs RHE). Thus, a strong dependence of HER activity with the upper inversion potential is manifest. By increasing the upper inversion potential (Fig. 8b), the absolute value of the current density at -50 mV vs RHE increases. Likewise, the current density during the forwards scan, related to the hydrogen oxidation reaction (HOR), measured at -20 mV, exhibits the same trend.

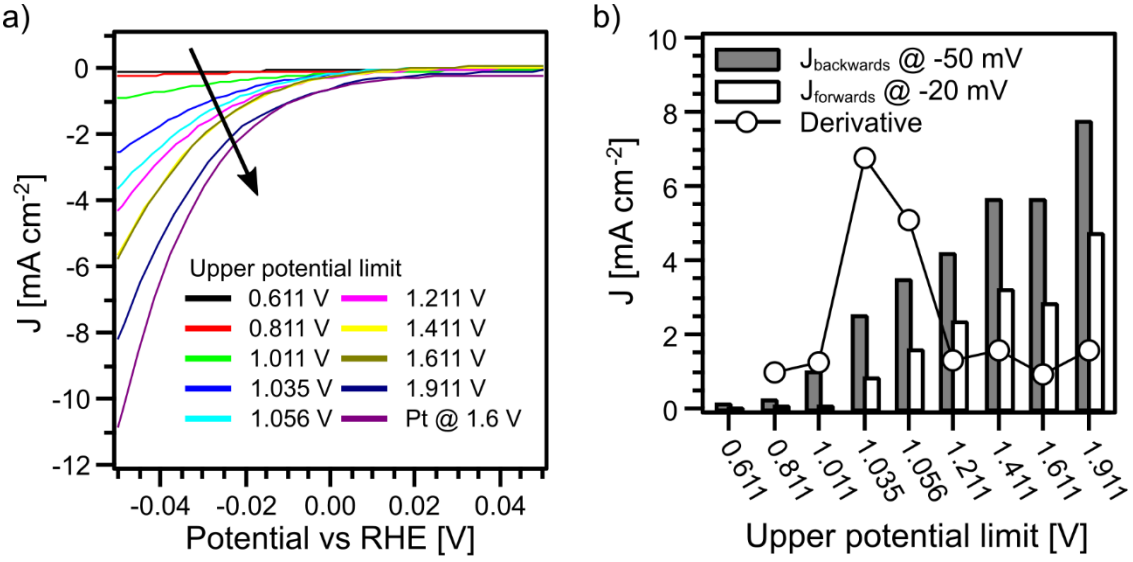

Figure 8. (a) Current density during the backwards scan (at 50 mV s^{-1}) as a function of the upper inversion potential limit. (b) Current density of the backwards scan at -50 mV (grey bars) and current density of the forwards scan at -20 mV (white bars). The derivative of the current density of the backwards scan at -50 mV is reported as white circles.

By inspecting the behaviour of the derivative of the current density at -50 mV as a function of the upper potential, it is evident that $PtSn_4$ behaves similarly to the Pt foil from 1.035 V as upper inversion potential. Increasing the upper potential limit, the current density still grows but with a lower slope. This suggests the key role of surface phenomena in HER promotion, starting around 1.0-1.1 V vs RHE, involving surface tin-oxide phases, whose presence on the substrate is evident by XPS and HREELS spectra in Figs. 2-4. To verify this phenomenon, we measured the Tafel slope for pristine sample and after a treatment at 1.035 V. As reported in Fig. 9, the slopes resulted to be 442 and 86 mV dec^{1}, respectively, thus confirming the improvement of HER kinetics after oxidation, in good agreement with theoretical findings.

However, we observed that performances of HER activity strikingly depend on surface preparation and treatments, thus clarifying that surface science can give a valuable contribution to $PtSn_4$-based catalysis.

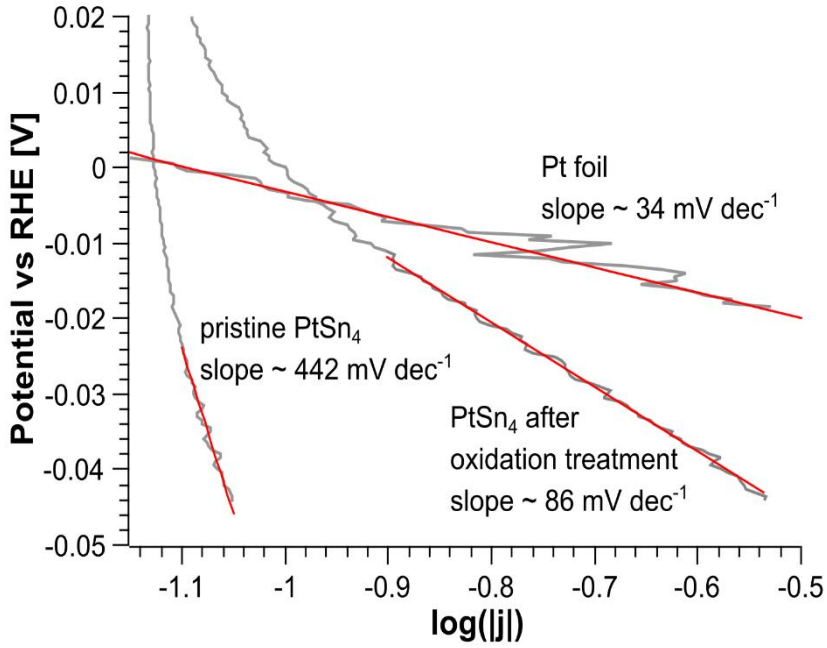

Figure 9. Tafel plot of pristine $PtSn_4$ and after the treatment at 1.035 V vs RHE, registered at 1 mV s^{-1}. For the sake of comparison, data for Pt foil are reported.

Finally, we have also certified the durability of $PtSn_4$-based electrodes by performing a chronomaperometric experiment at -44 mV vs RHE for 12 hours in 0.05 M H_2SO_4 (Fig. 10). The observed durability is evidently due to the passivation of the surface with tin-oxide phases.

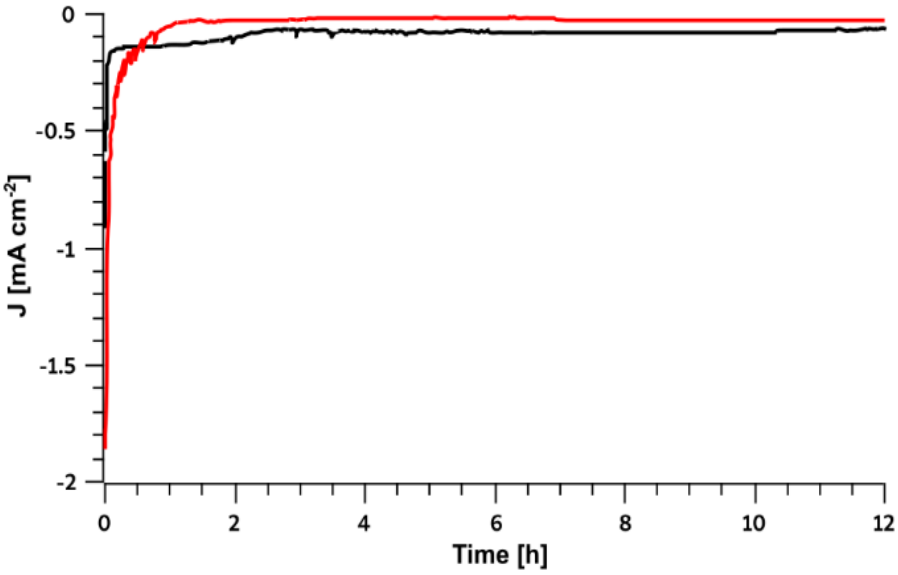

Figure 10. Chronomaperometric experiment at -44 mV vs RHE for 12 hours in 0.05 M H_2SO_4. Data for $PtSn_4$ and Pt are represented by black and red curves, respectively.

Conclusions

We have found that $PtSn_4$ is terminated with an atomic layer of Sn, which makes the surface fully tolerant to CO molecules. Oxidation of $PtSn_4$ surface occurs via the formation of a tin-oxide skin, whose thickness is limited to a few nanometers even after one year in air. However, surface oxidation is unexpectedly beneficial for catalysis.

Furthermore, the valence band does not show remarkable changes upon surface treatments and even after air exposure. Thus, we can assume that topological states of the bulk are robust against surface oxidation and this enables further applications of $PtSn_4$ in photonics and optoelectronics, to date completely unexplored.

Finally, we show that in the oxidized $PtSn_4$ surface the energy barrier of the Tafel step of HER decreases near to the value of the theoretical expectations for Heyrovsky step of HER on the Pt(111) surface. Moreover, with appropriate surface treatments is evident that is possible to optimize the catalytic activity of oxidized $PtSn_4$.

Besides, the interesting capability of a possibly achieved Pt-terminated surface by alternative methods (e.g. epitaxial growth) and the exclusive combination of the positions and distances of Pt centers should increase the selectivity of reactions, which is particularly relevant in organic chemistry.

Acknowledgments

GDO acknowledges funding from PON Ricerca e Innovazione 2014-2020 (project n. E12H1800010001) by MIUR.

Bibliography

[1] M.S. Bahramy, O.J. Clark, B.J. Yang, J. Feng, L. Bawden, J.M. Riley, I. Marković, F. Mazzola, V. Sunko, D. Biswas, S.P. Cooil, M. Jorge, J.W. Wells, M. Leandersson, T. Balasubramanian, J. Fujii, I. Vobornik, J.E. Rault, T.K. Kim, M. Hoesch, K. Okawa, M. Asakawa, T. Sasagawa, T. Eknapakul, W. Meevasana, P.D.C. King, Ubiquitous formation of bulk Dirac cones and topological surface states from a single orbital manifold in transition-metal dichalcogenides, Nat. Mater., 17 (2018) 21–28.
[2] M.Z. Hasan, C.L. Kane, Colloquium: Topological insulators, Rev. Mod. Phys., 82 (2010) 3045-3067.
[3] A. Thakur, K. Sadhukhan, A. Agarwal, Dynamic current-current susceptibility in three-dimensional Dirac and Weyl semimetals, Phys. Rev. B, 97 (2018) 035403.
[4] B. Singh, S. Mardanya, C. Su, H. Lin, A. Agarwal, A. Bansil, Spin-orbit coupling driven crossover from a starfruitlike nodal semimetal to Dirac and Weyl semimetal state in CaAuAs, Phys. Rev. B, 98 (2018) 085122.
[5] B. Singh, B. Ghosh, C. Su, H. Lin, A. Agarwal, A. Bansil, Topological Hourglass Dirac Semimetal in the Nonpolar Phase of Ag_2BiO_3, Phys. Rev. Lett., 121 (2018) 226401.
[6] I. Vobornik, U. Manju, J. Fujii, F. Borgatti, P. Torelli, D. Krizmancic, Y.S. Hor, R.J. Cava, G. Panaccione, Magnetic proximity effect as a pathway to spintronic applications of topological insulators, Nano Lett., 11 (2011) 4079-4082.
[7] F.D.M. Haldane, Nobel Lecture: Topological quantum matter, Rev. Mod. Phys., 89 (2017) 040502.
[8] H. Chen, W. Zhu, D. Xiao, Z. Zhang, CO oxidation facilitated by robust surface states on Au-covered topological insulators, Phys. Rev. Lett., 107 (2011) 056804.
[9] A. Politano, G. Chiarello, Z. Li, V. Fabio, L. Wang, L. Guo, X. Chen, D.W. Boukhvalov, Toward the effective exploitation of topological phases of matter in catalysis: chemical reactions at the surfaces of NbAs and TaAs Weyl semimetals, Adv. Funct. Mater., 28 (2018) 1800511.
[10] A. Politano, G. Chiarello, C.-N. Kuo, C.S. Lue, R. Edla, P. Torelli, V. Pellegrini, D.W. Boukhvalov, Tailoring the Surface Chemical Reactivity of Transition-Metal Dichalcogenide $PtTe_2$ Crystals, Advanced Functional Materials, 28 (2018) 1706504.
[11] Z.p. Xiang, H.q. Deng, P. Peljo, Z.y. Fu, S.l. Wang, D. Mandler, G.q. Sun, Z.x. Liang, Electrochemical Dynamics of a Single Platinum Nanoparticle Collision Event for the Hydrogen Evolution Reaction, Angew. Chem., 130 (2018) 3522-3526.
[12] J. Greeley, I. Stephens, A. Bondarenko, T.P. Johansson, H.A. Hansen, T. Jaramillo, J. Rossmeisl, I. Chorkendorff, J.K. Nørskov, Alloys of platinum and early transition metals as oxygen reduction electrocatalysts, Nature Chem., 1 (2009) 552.
[13] K. Ding, A. Gulec, A.M. Johnson, N.M. Schweitzer, G.D. Stucky, L.D. Marks, P.C. Stair, Identification of active sites in CO oxidation and water-gas shift over supported Pt catalysts, Science, 350 (2015) 189-192.
[14] R. Subbaraman, D. Tripkovic, D. Strmcnik, K.-C. Chang, M. Uchimura, A.P. Paulikas, V. Stamenkovic, N.M. Markovic, Enhancing hydrogen evolution activity in water splitting by tailoring Li^+-$Ni(OH)_2$-Pt interfaces, Science, 334 (2011) 1256-1260.
[15] R. Sari, S. Hammoudeh, U. Soytas, Dynamics of oil price, precious metal prices, and exchange rate, Energy Economics, 32 (2010) 351-362.
[16] E. Alonso, F.R. Field, R.E. Kirchain, Platinum availability for future automotive technologies, Environ. Sci. Technol., 46 (2012) 12986-12993.
[17] M. Shao, J.H. Odell, A. Peles, D. Su, The role of transition metals in the catalytic activity of Pt alloys: quantification of strain and ligand effects, Chem. Commun., 50 (2014) 2173-2176.
[18] A. Moscu, Y. Schuurman, L. Veyre, C. Thieuleux, F. Meunier, Direct evidence by in situ IR CO monitoring of the formation and the surface segregation of a Pt-Sn alloy, Chem. Commun., 50 (2014) 8590-8592.
[19] C. Kong, S. Min, G. Lu, Robust Pt-Sn alloy decorated graphene nanohybrid cocatalyst for photocatalytic hydrogen evolution, Chem. Commun., 50 (2014) 9281-9283.
[20] A.W. Hauser, J. Gomes, M. Bajdich, M. Head-Gordon, A.T. Bell, Subnanometer-sized Pt/Sn alloy cluster catalysts for the dehydrogenation of linear alkanes, Phys. Chem. Chem. Phys., 15 (2013) 20727-20734.
[21] C.T. Hsieh, Y.Y. Liu, W.Y. Chen, Y.H. Hsieh, Electrochemical activity and durability of Pt-Sn alloys on carbon-based electrodes prepared by microwave-assisted synthesis, Int. J. Hydrogen Energy, 36 (2011) 15766-15774.

[22] J.F. Kuhmann, C.-H. Chiang, P. Harde, F. Reier, W. Österle, I. Urban, A. Klein, Pt thin-film metallization for FC-bonding using SnPb60/40 solder bump metallurgy, Materials Science and Engineering: A, 242 (1998) 22-25.
[23] Z. Ma, S. Belyakov, K. Sweatman, T. Nishimura, C. Gourlay, Harnessing heterogeneous nucleation to control tin orientations in electronic interconnections, Nat. Commun., 8 (2017) 1916.
[24] B. Kempf, S. Schmauder, Thermodynamic modelling of precious metals alloys, Gold Bull., 31 (1998) 51-57.
[25] M.S. Kumar, D. Chen, A. Holmen, J.C. Walmsley, Dehydrogenation of propane over Pt-SBA-15 and Pt-Sn-SBA-15: Effect of Sn on the dispersion of Pt and catalytic behavior, Catal. Today, 142 (2009) 17-23.
[26] Y.-J. Leng, X. Wang, I.-M. Hsing, Assessment of CO-tolerance for different Pt-alloy anode catalysts in a polymer electrolyte fuel cell using ac impedance spectroscopy, J. Electroanal. Chem., 528 (2002) 145-152.
[27] X. Wang, I.-M. Hsing, Kinetics investigation of H2/CO electro-oxidation on carbon supported Pt and its alloys using impedance based models, J. Electroanal. Chem., 556 (2003) 117-126.
[28] A. Moscu, Y. Schuurman, L. Veyre, C. Thieuleux, F. Meunier, Direct evidence by in situ IR CO monitoring of the formation and the surface segregation of a Pt–Sn alloy, Chem. Commun., 50 (2014) 8590-8592.
[29] H. Okamoto, Pt-Sn (platinum-tin), J. Phase Equilib., 24 (2003) 198-198.
[30] Y. Wu, L.-L. Wang, E. Mun, D.D. Johnson, D. Mou, L. Huang, Y. Lee, S.L. Bud'ko, P.C. Canfield, A. Kaminski, Dirac node arcs in $PtSn_4$, Nat. Phys., 12 (2016) 667-671.
[31] E. Mun, H. Ko, G.J. Miller, G.D. Samolyuk, S.L. Bud'ko, P.C. Canfield, Magnetic field effects on transport properties of $PtSn_4$, Phys. Rev. B, 85 (2012) 035135.
[32] G. Li, C. Fu, W. Shi, L. Jiao, J. Wu, Q. Yang, R. Saha, M.E. Kamminga, A.K. Srivastava, E. Liu, A.N. Yazdani, N. Kumar, J. Zhang, G.R. Blake, X. Liu, M. Fahlman, S. Wirth, G. Auffermann, J. Gooth, S. Parkin, V. Madhavan, X. Feng, Y. Sun, C. Felser, Dirac Nodal Arc Semimetal $PtSn_4$: An Ideal Platform for Understanding Surface Properties and Catalysis for Hydrogen Evolution, Angew. Chem., 58 (2019) 13107-13112.
[33] A.J. Erdt, C. Gutsche, U.E.A. Fittschen, H. Borchert, J. Parisi, J. Kolny-Olesiak, Control of crystallographic phases and surface characterization of intermetallic platinum tin nanoparticles, CrystEngComm, 21 (2019) 3363-3373.
[34] S. Doniach, M. Sunjic, Many-electron singularity in X-ray photoemission and X-ray line spectra from metals, J. Phys. C, 3 (1970) 285.
[35] I. Horcas, R. Fernández, J.M. Gómez-Rodríguez, J. Colchero, J. Gómez-Herrero, A.M. Baro, WSXM: A software for scanning probe microscopy and a tool for nanotechnology, Rev. Sci. Instrum., 78 (2007) 013705.
[36] P. Giannozzi, S. Baroni, N. Bonini, M. Calandra, R. Car, C. Cavazzoni, D. Ceresoli, G.L. Chiarotti, M. Cococcioni, I. Dabo, A. Dal Corso, S. de Gironcoli, S. Fabris, G. Fratesi, R. Gebauer, U. Gerstmann, C. Gougoussis, A. Kokalj, L. Michele, L. Martin-Samos, N. Marzari, F. Mauri, R. Mazzarello, S. Paolini, A. Pasquarello, L. Paulatto, C. Sbraccia, S. Scandolo, G. Sclauzero, A.P. Seitsonen, A. Smogunov, P. Umari, R.M. Wentzcovitch, QUANTUM ESPRESSO: a modular and open-source software project for quantum simulations of materials, Journal of Physics: Condensed Matter, 21 (2009) 395502.
[37] J.P. Perdew, K. Burke, M. Ernzerhof, Generalized Gradient Approximation Made Simple, Physical Review Letters, 77 (1996) 3865-3868.
[38] V. Barone, M. Casarin, D. Forrer, M. Pavone, M. Sambi, A. Vittadini, Role and effective treatment of dispersive forces in materials: Polyethylene and graphite crystals as test cases, Journal of Computational Chemistry, 30 (2009) 934-939.
[39] D. Vanderbilt, Soft self-consistent pseudopotentials in a generalized eigenvalue formalism, Phys. Rev. B, 41 (1990) 7892-7895.
[40] K. Schubert, U. Rösler, Kristallstruktur von $PtSn_4$, Zeitschrift für Naturforschung A, 5 (1950) 127-127.
[41] Q. Li, X. Zhang, H. Liu, H. Wang, M. Zhang, Q. Li, Y. Ma, Structural and mechanical properties of platinum carbide, Inorg. Chem., 53 (2014) 5797-5802.
[42] B. Künnen, D. Niepmann, W. Jeitschko, Structure refinements and some properties of the transition metal stannides Os3Sn7, Ir5Sn7, Ni0.402(4)Pd0.598Sn4, α-PdSn2 and PtSn4, Journal of Alloys and Compounds, 309 (2000) 1-9.
[43] O. Matz, M. Calatayud, Breaking H2 with CeO2: Effect of Surface Termination, ACS Omega, 3 (2018) 16063-16073.

[44] D.J. Miller, H. Öberg, S. Kaya, H. Sanchez Casalongue, D. Friebel, T. Anniyev, H. Ogasawara, H. Bluhm, L.G.M. Pettersson, A. Nilsson, Oxidation of Pt(111) under Near-Ambient Conditions, Phys. Rev. Lett., 107 (2011) 195502.
[45] I. Píš, E. Magnano, S. Nappini, F. Bondino, Under-cover stabilization and reactivity of a dense carbon monoxide layer on Pt(111), Chem. Sci., 10 (2019) 1857-1865.
[46] S. Nappini, I. Píš, T.O. Menteş, A. Sala, M. Cattelan, S. Agnoli, F. Bondino, E. Magnano, Formation of a Quasi-Free-Standing Single Layer of Graphene and Hexagonal Boron Nitride on Pt(111) by a Single Molecular Precursor, Adv. Funct. Mater., 26 (2016) 1120-1126.
[47] S. Hsieh, T. Matsumoto, M. Batzill, B.E. Koel, Structural and chemical properties of a c(2x2)-Ti/Pt(100) second-layer alloy: A probe of strong ligand effects on surface Pt atoms, Phys. Rev. B, 68 (2003) 205417.
[48] H. Igarashi, T. Fujino, Y. Zhu, H. Uchida, M. Watanabe, CO tolerance of Pt alloy electrocatalysts for polymer electrolyte fuel cells and the detoxification mechanism, Phys. Chem. Chem. Phys., 3 (2001) 306-314.
[49] M. Fondell, M. Gorgoi, M. Boman, A. Lindblad, An HAXPES study of Sn, SnS, SnO and SnO_2, J. Electron Spectrosc. Relat. Phenom., 195 (2014) 195-199.
[50] Y. Jugnet, D. Loffreda, C.l. Dupont, F.o. Delbecq, E. Ehret, F.J. Cadete Santos Aires, B.S. Mun, F. Aksoy Akgul, Z. Liu, Promoter Effect of Early Stage Grown Surface Oxides: A Near-Ambient-Pressure XPS Study of CO Oxidation on PtSn Bimetallics, J. Phys. Chem. Lett., 3 (2012) 3707-3714.
[51] M. Kwoka, L. Ottaviano, M. Passacantando, S. Santucci, G. Czempik, J. Szuber, XPS study of the surface chemistry of L-CVD SnO2 thin films after oxidation, Thin Solid Films, 490 (2005) 36-42.
[52] H. Ishitobi, Y. Kawatsu, Y. Kudo, N. Nakagawa, Maximized specific activity for the methanol electrooxidation by the optimized PtRu-TiO_2-carbon nano-composite structure, Int. J. Hydrogen Energy, 44 (2019) 30743-30753.
[53] E. Ding, K.L. More, T. He, Preparation and characterization of carbon-supported PtTi alloy electrocatalysts, J. Power Sources, 175 (2008) 794-799.
[54] Z. Luo, J. Lu, C. Flox, R. Nafria, A. Genç, J. Arbiol, J. Llorca, M. Ibáñez, J.R. Morante, A. Cabot, Pd_2Sn [010] nanorods as a highly active and stable ethanol oxidation catalyst, J. Mater. Chem. A, 4 (2016) 16706-16713.
[55] Z. Liu, L. Ma, J. Zhang, K. Hongsirikarn, J.G. Goodwin, Pt Alloy Electrocatalysts for Proton Exchange Membrane Fuel Cells: A Review, Catal. Rev., 55 (2013) 255-288.
[56] M. Vandichel, A. Moscu, H. Grönbeck, Catalysis at the rim: A mechanism for low temperature CO oxidation over Pt_3Sn, ACS Catalysis, 7 (2017) 7431-7441.
[57] K. Balakrishnan, J. Schwank, A chemisorption and XPS study of bimetallic Pt-Sn/Al_2O_3 catalysts, J. Catal., 127 (1991) 287-306.
[58] W. Wan, Y. Ge, Y. Liu, Strong phonon anharmonicity and low thermal conductivity of monolayer tin oxides driven by lone-pair electrons, Appl. Phys. Lett., 114 (2019) 031901.
[59] P.R. Kidambi, B.C. Bayer, R. Blume, Z.-J. Wang, C. Baehtz, R.S. Weatherup, M.-G. Willinger, R. Schloegl, S. Hofmann, Observing graphene grow: catalyst–graphene interactions during scalable graphene growth on polycrystalline copper, Nano Lett., 13 (2013) 4769-4778.
[60] L.-Å. Näslund, Hydrogenation of O and OH on Pt (111): A comparison between the reaction rates of the first and the second hydrogen addition steps, J. Chem. Phys., 140 (2014) 104701.
[61] T. Schiros, L.-Å. Näslund, K. Andersson, J. Gyllenpalm, G. Karlberg, M. Odelius, H. Ogasawara, L.G. Pettersson, A. Nilsson, Structure and bonding of the water− hydroxyl mixed phase on Pt (111), J. Phys. Chem. C, 111 (2007) 15003-15012.
[62] L. Liu, M. An, P. Yang, J. Zhang, Superior cycle performance and high reversible capacity of SnO2/graphene composite as an anode material for lithium-ion batteries, Sci. Rep., 5 (2015) 9055.
[63] M. Batzill, K. Katsiev, J.M. Burst, Y. Losovyj, W. Bergermayer, I. Tanaka, U. Diebold, Tuning surface properties of SnO_2(101) by reduction, J. Phys. Chem. Solids, 67 (2006) 1923-1929.
[64] I.G. Casella, E. Desimoni, XPS, SEM and electrochemical characterization of a platinum-based glassy carbon modified electrode. Electrocatalytic oxidation of ethanol in acidic medium, Electroanalysis, 8 (1996) 447-453.

[65] K.I.B. Eguiluz, G.R.P. Malpass, M.M.S. Pupo, G.R. Salazar-Banda, L.A. Avaca, Synthesis, Characterization, and Electrocatalytic Activity toward Methanol Oxidation of Carbon-Supported Ptx−(RuO2−M)1−x Composite Ternary Catalysts (M = CeO2, MoO3, or PbOx), Energy Fuels, 24 (2010) 4012-4024.
[66] G. Chiarello, A.R. Marino, V. Formoso, A. Politano, The adsorption and co-adsorption of oxygen and carbon monoxide on $Pt_3Ni(111)$: A vibrational study, J. Chem. Phys., 134 (2011) 224705.
[67] A. Atli, M. Abon, P. Beccat, J. Bertolini, B. Tardy, Carbon monoxide adsorption on a $Pt_{80}Fe_{20}(111)$ single-crystal alloy, Surf. Sci., 302 (1994) 121-125.
[68] J. Liu, F.R. Lucci, M. Yang, S. Lee, M.D. Marcinkowski, A.J. Therrien, C.T. Williams, E.C.H. Sykes, M. Flytzani-Stephanopoulos, Tackling CO poisoning with single-atom alloy catalysts, J. Am. Chem. Soc., 138 (2016) 6396-6399.
[69] A. Ponrouch, S. Garbarino, D. Guay, Effect of the nanostructure on the CO poisoning rate of platinum, Electrochem. Commun., 11 (2009) 834-837.
[70] C. Farrell, C. Gardner, M. Ternan, Experimental and modelling studies of CO poisoning in PEM fuel cells, J. Power Sources, 171 (2007) 282-293.
[71] K. Matsuoka, Y. Iriyama, T. Abe, M. Matsuoka, Z. Ogumi, Electro-oxidation of methanol and ethylene glycol on platinum in alkaline solution: Poisoning effects and product analysis, Electrochim. Acta, 51 (2005) 1085-1090.
[72] E. Herrero, K. Franaszczuk, A. Wieckowski, Electrochemistry of methanol at low index crystal planes of platinum: an integrated voltammetric and chronoamperometric study, J. Phys. Chem., 98 (1994) 5074-5083.
[73] J. Wang, Y. Wang, K. Jacobi, The molecular adsorption of CO on the Ru(1120) surface, Surf. Sci., 482 (2001) 153-159.
[74] H. Ibach, Electron-Energy-Loss Spectroscopy - the Vibration Spectroscopy of Surfaces, Surf. Sci., 299 (1994) 116-128.
[75] A. Politano, G. Chiarello, Vibrational investigation of catalyst surfaces: change of the adsorption site of CO molecules upon coadsorption, The Journal of Physical Chemistry C, 115 (2011) 13541-13553.

***Credit Author Statement**

Credit author statement

The project was conceived and coordinated by GDO and AP; DFT calculations were performed by DWB; electrochemical tests were done by AM and JFi under the coordination of FV; RE and GDO acquired XPS data, under the supervision of AP and PT, while XPS data analysis was done by SN; LEED experiments were done by PT and JFu; STM was performed by JF with the scientific collaboration of LO; samples were grown by CNK under the supervision of CSL and AP; HREELS experiments were performed by AP and GDO and analyzed by AP and GDO; XRD analysis was carried out by CSL and CNK. The paper was written by GDO and AP with the participation of DWB, SN and AM-JFi-FV for theoretical, XPS and electrochemistry parts, respectively.